Accepted Manuscript

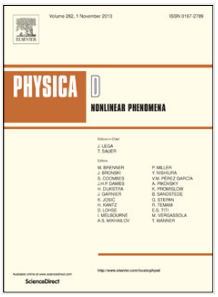

Three-dimensional forced-damped dynamical systems with rich dynamics: Bifurcations, chaos and unbounded solutions

Tomoyuki Miyaji, Hisashi Okamoto, Alex D.D. Craik

PII: S0167-2789(15)00168-2
DOI: http://dx.doi.org/10.1016/j.physd.2015.09.001
Reference: PHYSD 31674

To appear in: *Physica D*

Received date: 26 November 2014
Revised date: 31 August 2015
Accepted date: 1 September 2015

Please cite this article as: T. Miyaji, H. Okamoto, A.D.D. Craik, Three-dimensional forced-damped dynamical systems with rich dynamics: Bifurcations, chaos and unbounded solutions, *Physica D* (2015), http://dx.doi.org/10.1016/j.physd.2015.09.001

- Rich orbit structures of some three-dimensional dynamical systems are studied.
- Computational, analytical and asymptotic methods are employed.
- Four-leaf structure, bounded and unbounded orbits coexist.
- Three distinct period-doubling cascades to chaos are found.
- The structure changes drastically depending on damping and forcing parameters.

Three-dimensional forced-damped dynamical systems with rich dynamics: bifurcations, chaos and unbounded solutions

Tomoyuki Miyaji[a,1,*], Hisashi Okamoto[b], Alex D. D. Craik[c]

[a] *Organization for the Strategic Coordination of Research and Intellectual Properties, Meiji University, 4-21-1 Nakano, Nakano-ku, Tokyo 164-8525, Japan*
[b] *Research Institute for Mathematical Sciences, Kyoto University, Kyoto 606-8502, Japan*
[c] *School of Mathematics & Statistics, University of St Andrews, St. Andrews, KY16 9SS, Scotland, UK*

Abstract

We consider certain autonomous three-dimensional dynamical systems that can arise in mechanical and fluid-dynamical contexts. Extending a previous study in Craik & Okamoto, Physica D 164 (2002) 168–186, to include linear forcing and damping, we find that the four-leaf structure discovered in that paper, and unbounded orbits, persist, but may now be accompanied by three distinct period-doubling cascades to chaos, and by orbits that approach stable equilibrium points. This rich structure is investigated both analytically and numerically, distinguishing three main cases determined by the damping and forcing parameter values.

Keywords: three-dimensional dynamical system, period-doubling cascades to chaos, asymptotic analysis, Lyapunov function

2010 MSC: 34A34, 37C10

*Corresponding author
Email addresses: tmiyaji@meiji.ac.jp (Tomoyuki Miyaji), okamoto@kurims.kyoto-u.ac.jp (Hisashi Okamoto), addc@st-andrews.ac.uk (Alex D. D. Craik)
[1] *Tel:*+81-3-5343-8375

1. Introduction

The following conservative dynamical system was studied in [1]:

$$\dot{x} = ayz + bz + cy, \quad \dot{y} = dzx + ex + fz, \quad \dot{z} = gxy + hy + kx, \tag{1}$$

where $x(t)$, $y(t)$, $z(t)$ are real functions and the overdot denotes differentiation with respect to the time-like independent variable t, and the coefficients a to k are real constants. Our paper [1] (and [2] before that) showed that, despite their simple form, the solution structure of this system is quite rich. Similar but different systems are considered in [3, 4, 5, 6, 7].

If a, d, g are of the same sign, then the solution may blow up in finite time. Our standing assumption in this paper is that two of them are of differing sign from the third. Then it is elementary to prove that no solution blows up in finite time: see section 2 of [8]. Equations of this form arise in many branches of mechanics. See [1, 9, 10, 11, 12, 13, 14], particularly [1], where some physical background is explained.

The theory of dynamical systems in $\mathbb{R}^3$ has attracted very many researchers, but standard theories mostly concern systems in which all trajectories remain bounded at all times. Then, exotic behaviour is normally connected with the existence of homoclinic or heteroclinic orbits and of strange attractors. One might be forgiven for thinking that systems with mainly unbounded trajectories are relatively unimportant and uninteresting. However, our system arises in mechanics in a natural fashion and we proved in [1] that the system above has a class of interesting orbits. Also, our system has a 'sister' which arises in electric circuits and which possesses a chaotic orbit of four-leaf form, reminiscent of the non-chaotic orbit in [1]. This was considered by Pehlivan [15], and satisfies the following system of ordinary differential equations:

$$\dot{x} = yz - ax + y, \quad \dot{y} = bzx + x - ay, \quad \dot{z} = -bxy + cz, \tag{2}$$

where a, b, c are real constants. For certain values of a, b, c a chaotic orbit appears. The whole picture of bifurcations and chaotic attractors of the four-leaf

structure of (2) are studied in [8], where the origin of Pehlivan's chaotic orbit was explained by period-doubling cascades. When a and c are zero, system (2) is just a special case of (1) and of (3) below; but inclusion of linear growth or damping terms in a and c fundamentally alters the dynamics. Below, we add such linear terms to (3) to study the resulting dynamics of this more general system, with the aim of connecting the previous studies [1] and [8].

Specifically, in (1), we restrict ourselves to the case where two of a, d, g are positive and the third is negative. (If, instead, one is positive and the other two negative, such cases may be converted by the transformation $(x, y, z) \mapsto (-x, -y, -z)$.) Without loss of generality, we may assume that a and g are positive and d is negative. Also, if $(x, y, z, t) \mapsto (Ax, By, Cz, Tt)$ is substituted and the positive constants A, B, C, T are suitably chosen, then we may set $a = 1, b = -1, g = 1$, obtaining

$$\dot{x} = yz + ay + bz, \quad \dot{y} = -zx + cx + dz, \quad \dot{z} = xy + hy + kx. \tag{3}$$

Here notations are changed and new a, b, etc. are introduced.

However, providing a comprehensive study of this system for general parameter values with added growth and damping is too great a task. Accordingly, we further restrict attention to an appropriate subclass of vector fields that we believe exhibits typical dynamical behaviour. Our chosen equations, with added damping and growth terms, are

$$\dot{X} = Y(Z - 1) + hX, \quad \dot{Y} = -Z(X - 1) - kY, \quad \dot{Z} = X(Y - 1) + hZ, \tag{4}$$

where either (Case A) $h < 0, k < 0$, or (Case B) $h > 0, k > 0$, or (Case C) $h < 0, k > 0$. Also, since we are mainly interested in cases where the phase volume is contracted, we assume hereafter that $2h - k < 0$ unless otherwise noted. If $(h, k) = (0, 0)$, (4) reverts to (10) below in subsection 2.1. The latter, which was introduced in [1], is not a chaotic system: most solutions are unbounded and have spring-like appearance with or without bending at a right angle; and many such orbits take a four-leaf form for a considerable time.

Below, we investigate these three distinct cases separately. Case A is the

most interesting and challenging. It exhibits three different types of chaotic attractor, one of which has the expected 'four-leaf' form: transition to chaos is by repeated period-doubling bifurcations. In Case B, almost all orbits approach infinity: we present an asymptotic analysis of these that agrees with our computations. In Case C, in which the terms in h and k are both damping, solutions remain bounded, and may approach one of several fixed points or a limit cycle.

The present paper consists of seven sections. Before considering what happens when the terms in h and k are introduced, we offer some preliminary remarks about conservative systems in section 2. Then the governing equations are introduced in section 3. Case A is studied in section 4. Case B and Case C are considered in sections 5 and 6, respectively. The final section is devoted to some further remarks.

2. Preliminaries: conservative systems

Before we study chaotic dynamical systems, we recall some properties of conservative systems. We begin with the simplest case, a system without linear terms.

$$\dot{x} = yz, \qquad \dot{y} = -xz, \qquad \dot{z} = xy. \tag{5}$$

This is a special case of the equations for a freely-rotating rigid body, first given by Euler [16]. Sufficiently large solutions of (3) may clearly be regarded as perturbations from (5). Therefore we recall some facts about (5). First, note that x^2+y^2, y^2+z^2, and x^2-z^2 are conserved, whence $x^2+2y^2+z^2$ is conserved. For each $R>0$, the ellipsoid $x^2+2y^2+z^2=R^2$ has equilibria

$$(x,y,z) = (\pm R, 0, 0), \qquad (x,y,z) = (0, \pm R/\sqrt{2}, 0), \qquad (x,y,z) = (0,0,\pm R).$$

The first and the third are stable (centres). The points $(0, \pm R/\sqrt{2}, 0)$ are saddles, and are mutually connected by heteroclinic orbits: See Figure 1. The heteroclinic orbits, given by $x = \pm z, x^2+2y^2+z^2 = R^2$, are half ellipses. The ellipsoid, except for the heteroclinic orbits and equilibria, is covered by closed orbits, which can be written in terms of elliptic functions. Two heteroclinic

orbits on the ellipsoidal surface can produce a homoclinic orbit if perturbations are added, as we will soon see. Since there is an infinite number of ellipsoids with different R, we may expect perturbations to produce interesting solution structures. The invariant set $x = \pm z$ consists of four leaves of half planes, and is filled with heteroclinic orbits (Figure 1(b)). We will see a similar structure later in this paper.

The following perturbation is now added:

$$\dot{x} = yz + az, \qquad \dot{y} = -xz, \qquad \dot{z} = xy + bx. \tag{6}$$

This is still a conservative system. In fact, if we choose two constants A and B such that $A+B = 1, Aa+Bb = 0$, then $Ax^2+y^2+Bz^2$ is a constant of motion. Since $A = b/(b-a), B = -a/(b-a)$, both A and B are positive if and only if $ab < 0$. If $a = b$, then $x^2 - z^2$ is a constant of motion. If $ab > 0$ but $a \neq b$, then the constant of motion $Ax^2 + y^2 + Bz^2$ is a hyperboloid of revolution.

If $A = B = 1/2$, then $x\dot{x} + 2y\dot{y} + z\dot{z} = (a+b)xz$, so setting $b = -a$ gives a conservative system with $x^2 + 2y^2 + z^2$ constant. Rescaling $(x, y, z, t) = (\sigma X, \sigma Y, \sigma Z, T/\sigma)$ with a certain σ gives

$$\dot{X} = (Y+1)Z, \qquad \dot{Y} = -XZ, \qquad \dot{Z} = X(Y-1). \tag{7}$$

We set $X^2 + 2Y^2 + Z^2 = R^2$. Fixed points are $(0, \pm R/\sqrt{2}, 0)$, $(0, -1, \pm(R^2 - 1)^{1/2})$, $(\pm(R^2-1)^{1/2}, 1, 0)$. The latter two exist only if $R \geq 1$.

Since $X\dot{X} - Z\dot{Z} = 2XZ = -2\dot{Y}$, another constant of the motion is

$$X^2 - Z^2 + 4Y = Q, \tag{8}$$

say. Eliminating X^2 and Z^2 in turn gives a pair of circular cylinders. X, Y, Z can then be represented parametrically in terms of sines and cosines of an angle, if required. The phase portrait on the ellipsoid is drawn in Figure 2.

The four fixed points

$$(0, -1, \pm(R^2-1)^{1/2}), \qquad (\pm(R^2-1)^{1/2}, 1, 0)$$

are centres (when they exist). Those at $(0, \pm R/\sqrt{2}, 0)$ are a saddle when $R^2 > 1$ and a centre when $R^2 < 1$.

(7) is invariant under the transformation $(X, Y, Z) \mapsto (Z, -Y, -X)$. The big difference between (7) and (5) is that solutions emerging from either saddle point at $(0, \pm R/\sqrt{2}, 0)$ no longer pass through the opposite saddle point. Instead, there is a band of 'four-leaf' solutions, as well as the simpler "precessing" solutions centred around the other fixed points. In other words (5) have heteroclinic orbits, while (7) have homoclinic orbits obtained by setting $Q = \pm 2R$ in (8). These four-leaf solutions tend to the heteroclinic orbit appearing in (5) if R increases indefinitely. If R is not large, they look more like a seam of a baseball or a tennis ball than four-leaf. If $R^2 < 1$, all solutions are of "precessing" type, around the only two centres at $(0, \pm R/\sqrt{2}, 0)$. Some trajectories are plotted in Figure 2.

There are more general equations that conserve "energy": $x^2 + 2y^2 + z^2 =$ const. These are:

$$\dot{x} = yz + az + 2cy, \qquad \dot{y} = -xz - cx + dz, \qquad \dot{z} = xy - ax - 2dy. \tag{9}$$

The case above has $c = d = 0$. Cases with $a = d = 0$ or with $a = c = 0$ seem to be broadly similar to that with $c = d = 0$: all have four centres and two saddle points. Cases where at least two of a, b, c are non-zero are harder to analyse, as locations of the fixed points are more complicated: Numerical tests show qualitatively similar phase portraits, although they are much less symmetric. Since they are topologically similar to those in Figure 2, figures are omitted.

The equations in Sect. 6 of Craik & Okamoto [1] are

$$\dot{X} = Y(Z-1), \qquad \dot{Y} = -Z(X-1), \qquad \dot{Z} = X(Y-1), \tag{10}$$

by which the present study is motivated. These have particular growing solutions

$$(X, Y, Z) = (1, 0, -t), \qquad (-t, 1, 0), \qquad (0, t, 1) \qquad (-\infty < t < \infty).$$

We may suppress this growth with t by adding constants to the right hand sides:

$$\dot{X} = Y(Z-1) + 1, \qquad \dot{Y} = -Z(X-1) - 1, \qquad \dot{Z} = X(Y-1) + 1. \tag{11}$$

This system does not fall into the class described by (1). But since its phase portrait has some similarities with that above, we briefly consider it. (11) is now conservative with constants of motion, e.g.

$$(X-2)^2+2(Y-1/2)^2+(Z+1)^2=R^2; \qquad (X-1)^2+Y^2+2Z=Q.$$

The first one gives rise to a family of ellipsoids, and the second that of paraboloids. Some examples of curves resulting from intersections of these surfaces are shown in Figure 3. The phase portrait on the ellipsoid $(X-2)^2+2(Y-1/2)^2+(Z+1)^2=R^2$ depends on R. If R is sufficiently small the ellipsoid has two and only two equilibria. All other orbits are then periodic. If R is large, there are four centres and two saddles, which accompany two homoclinic orbits. A simple computation shows that this change first happens if $R>3.9667\cdots$. The Y-coordinate of the equilibria are then determined by

$$(4W+1)(W^2+4W+2)=2R^2W^2 \qquad (W=Y^2-Y)$$

from which X and Z are readily obtained.

We may summarise this section in the following way. (3) is integrable for some parameters and can produce closed orbits of four-leaf or tennis ball shape. We will later see that some invariants with modifications will serve as Lyapunov functions for equilibria in the generalised system (4) above.

3. The governing equations

We now consider (4), which is an extension of the equations in (10). We study the following three cases: (Case A) $h<0,k<0$, (Case B) $h>0,k>0$, and (Case C) $h<0,k>0$. Since we are interested in the case where the phase volume is contracted, we assume in this section that $2h-k<0$ unless otherwise noted. This implies in particular that we ignore the remaining Case D, with $h>0,k<0$, in which both added terms are forcing: clearly, then all solution trajectories may go off to infinity, much as in [1] but with some distortion.

If $(h,k)=(0,0)$, (4) becomes (10). (10) is not a chaotic system, but most solutions are unbounded and have spring-like appearance with or without bending

at a right angle. Craik & Okamoto [1] found numerically an unstable periodic orbit of (10) which plays an important role in determining the direction of the orbits. This periodic orbit is reproduced in Figure 4. Later, Miyaji & Okamoto [17] proved rigorously the existence and local uniqueness of the unstable periodic orbit with the aid of interval arithmetic.

With the introduction of terms in h and k, we find chaotic orbits in Case A; but none in Case B for which orbits escape to infinity; and none in Case C, where all orbits enter an ellipsoidal region, as we will prove in section 6. In the next section we analyse (4) in Case A.

In the following analysis, we used AUTO-07p [18] to numerically compute bifurcating solutions. In the figures we use many abbreviations which are listed in Table 1

Table 1: Graph legend

`SE`	Stable Equilibrium	`LP`	Limit Point
`UE`	Unstable Equilibrium	`BP`	Bifurcation Point
`SC`	Stable Cycle	`PD`	Period Doubling bifurcation
`UC`	Unstable Cycle	`CP`	Cusp Point
`max(x)`	$\max\{x(t) \mid t > 0\}$	`BT`	Bogdanov-Takens bifurcation

4. Case A

In Case A, we found three different kinds of chaotic attractor that can exist together for the same values of h, k (Figure 5(d)). Depending on initial data, an orbit of (4) with $(h, k) = (-1.97, -1.1262)$, for example, tends to one of the three chaotic attractors, an equilibrium, a periodic orbit, or infinity. By chaotic we mean that the orbit has a positive Lyapunov exponent. Three typical examples of chaotic orbits are drawn in Figure 5. Figure 5(a) has a four-leaf shape. The largest Lyapunov exponent is $0.209, 0.071, 0.12$ for Figure 5(a), Figure 5(b), and

Figure 5(c), respectively. (We computed these values by a method using the QR factorization [19, Section V.C].)

The parameter region of (h, k) in which these three attractors coexist is found to be rather small. We could not find an attractor like Figure 5(c) when $h = -1.5$.

We now look more closely at the three chaotic attractors separately from dynamical systems viewpoint. We begin with the four-leaf chaos.

4.1. Chaotic four-leaf attractors

The chaotic four-leaf attractor in Figure 5(a) appears as a result of a period-doubling cascade. For the sake of convenience, we fix $h = -1.5$ and regard k as a bifurcation parameter. There is a stable limit cycle of four-leaf form at $(h, k) = (-1.5, -1.1)$ as shown in Figure 6(a). This limit cycle indeed looks similar to the unstable orbit in Figure 4, and we explain their relation later in this section. As k increases, this limit cycle loses its stability by a period-doubling bifurcation. See Figure 6(b). With increasing k, a cascade of period-doubling bifurcations emerges. Figure 6 shows stable limit cycles of period 1, 2, 4, while Figure 7(a) shows a bifurcation diagram computed by AUTO. Figure 7(b) shows an orbit diagram.

Let k_n denote the n-th period-doubling bifurcation point for $n = 1, 2, \cdots$. The first nine k_n's are:

$$k_1 \approx -1.046324145005, \quad k_2 \approx -1.024987795333, \quad k_3 \approx -1.020644724412,$$
$$k_4 \approx -1.019725205679, \quad k_5 \approx -1.019528751781, \quad k_6 \approx -1.019486699386,$$
$$k_7 \approx -1.019477694058, \quad k_8 \approx -1.019475765439, \quad k_9 \approx -1.019475352390.$$

Following Feigenbaum [20], we define $\delta_n = (k_{n+1} - k_n)/(k_{n+2} - k_{n+1})$. We then obtain

$$\delta_1 \approx 4.912733423510, \quad \delta_2 \approx 4.723200044252, \quad \delta_3 \approx 4.680582778272,$$
$$\delta_4 \approx 4.671645941671, \quad \delta_5 \approx 4.669723971656, \quad \delta_6 \approx 4.669313603257,$$
$$\delta_7 \approx 4.669225622228.$$

The last value is very close to the Feigenbaum constant $\delta = 4.6692016\cdots$. Therefore Feigenbaum's theory can be applied to our problem and we expect the cascade to end at $k_\infty := \lim_{n\to\infty} k_n$ and chaotic orbits emerge for $k > k_\infty$. If we define $\tilde{k}_n$ by

$$(\tilde{k}_{n+1} - \tilde{k}_n)/(\tilde{k}_{n+2} - \tilde{k}_{n+1}) = \delta, \qquad \tilde{k}_2 = k_2, \quad \tilde{k}_3 = k_3,$$

Then $\lim_{n\to\infty} \tilde{k}_n = (\delta k_3 - k_2)/(\delta - 1) = -1.019461063$, which can be used for an approximate value of $\lim k_n$.

The four-leaf attractors are related to the unstable periodic orbit of (10) (Figure 4). Indeed, the periodic orbit in Figure 4 is connected to the one in Figure 6(a) by a family of periodic orbits. Starting from the unstable periodic orbit at $(h, k) = (0, 0)$, we compute in the following way. First, fix $h = 0$ and decrease k from $k = 0$. Figure 8(a) shows the bifurcation diagram. There is a limit point of the branch at $k \approx -0.224$. With this limit point as an initial point, we then compute, by AUTO, the path of limit points on the (h, k)-plane to obtain a curve C_{LP} of limit points. C_{LP} intersects the line $h = -1.5$ as shown in Figure 8(b). This intersection is the limit point appearing in Figure 7(a). From there we increase k to obtain the period-doubling bifurcation above. In this sense we may say that the unstable periodic orbit, which was discovered by [1] and was proved to exist by [17], is the origin of the four-leaf chaotic attractor.

4.2. Figure 5(b)

We now explain the origin of the chaotic attractor of Figure 5(b). We first determine equilibria of (4). They are either the origin or those given by a root of

$$h\{X(1-X) + hk\}^2 + (1-X)\{kX - X(1-X) - hk\} = 0.$$

The origin is unstable: The linearised matrix of (4) at the origin is

$$A = \begin{pmatrix} h & -1 & 0 \\ 0 & -k & 1 \\ -1 & 0 & h \end{pmatrix}, \tag{12}$$

whose trace $2h - k$ is negative by our assumption. Its determinant is $\det A = 1-h^2k$, which is positive since we are now assuming that $h < 0, k < 0$. Therefore the index of the equilibrium $(0, 0, 0)$ is one, and it has a one-dimensional unstable manifold.

Figure 9, where $h = -1.5$ is fixed and k is varied, is a bifurcation diagram for two of the four nontrivial equilibria. (Two others do not produce a bifurcation and seem to have no influence on the chaotic attractors in this parameter region. They do have bifurcations for other parameters, though.) Each equilibria undergoes a Hopf bifurcation, and stable limit cycles bifurcate. The period of the limit cycle increases as k tends to a certain value. It seems that each branch of limit cycles terminates at a homoclinic orbit. (In other words, the limit cycles bifurcate from a homoclinic orbit.) Figure 10(a) shows limit cycles at some values of k. A homoclinic orbit exists at $k = -0.738131$ and another at $k = -1.06355$.

When $k = -0.738131$ and $k = -1.06355$, the origin is a saddle-focus with one-dimensional unstable manifold. Let μ_1, μ_2, and μ_3 be the linearised eigenvalues at the origin, where μ_1 is real and the others are a complex conjugate pair. Šhil'nikov's theorem in [21] implies that a Smale horseshoe may appear in a neighbourhood of an orbit homoclinic to a saddle-focus if $\sigma := \mu_1 + \mathrm{Re}(\mu_2)$ is positive. However, in our case, it turns out that $\sigma < 0$. Therefore these homoclinic orbits at $k = -0.738131$ and $k = -1.06355$ are not immediately connected to chaos.

The reason for the occurrence of chaotic attractors in Figure 5(b) is involved. Homoclinic orbits other than those above bifurcate and these new homoclinic orbits produce periodic orbits. Figure 11 shows orbit diagrams for $h = -1.5$ and $h = -1.7$, both of which clearly indicate a period-doubling cascade to chaos. By Figure 12, we see that the cycle at $h = -1.5$ which undergoes a period-doubling bifurcation is different from that at -1.7. Those are connected to the chaotic attractor in Figure 5(b). Since numerical data for this transition to chaos require more pages, we leave the study to the forthcoming paper [22].

4.3. Figure 5(c)

Figure 5(c) appears as a result of a period-doubling cascade. Let $h = -2.0$ and let k vary. Figure 13 shows several periodic orbits. Figure 14 shows the bifurcation diagram (a) and the orbit diagram (b). Successive period-doubling bifurcations are clearly observed.

As we have done in subsection 4.1, let k_n denote the n-th period-doubling bifurcation point for $n = 1, 2, \cdots$. The first nine k_n's are:

$$k_1 \approx -1.136662090633, \quad k_2 \approx -1.131277684733, \quad k_3 \approx -1.130024334242,$$
$$k_4 \approx -1.129752498281, \quad k_5 \approx -1.129694088442, \quad k_6 \approx -1.129681571055,$$
$$k_7 \approx -1.129678889831, \quad k_8 \approx -1.129678315578, \quad k_9 \approx -1.129678192590.$$

If we define $\delta_n = (k_{n+1} - k_n)/(k_{n+2} - k_{n+1})$, we obtain $\delta_7 \approx 4.66917268568132$, which is very close to the Feigenbaum constant.

4.4. Non-chaotic orbits

Figure 15 shows several orbits which converge to a stable equilibrium of (4) with $(h, k) = (-1.5, -0.1)$. Some orbits trace a helical curve and some others trace a four-leaf before converging to an equilibrium.

As Figure 16 demonstrates, unbounded orbits can exist. These tend to infinity, forming a four-leaf shape. Such unbounded orbits exist simultaneously with the bounded chaotic orbits as shown in Figure 5(a).

5. Case B

Here, we find no chaotic attractor, though it is not easy to predict asymptotic behaviour of orbits for all (h, k): for instance, if both h and k are small, the unstable periodic orbit of (10) in Figure 4 persists since it is hyperbolic. However, if (h, k) is not close to the origin, solutions seem to tend always towards infinity despite the condition $2h - k < 0$. Figure 17 shows four trajectories for $h = 0.3, k = 2$. Two of them tend to $(1, 0, -\infty)$ as $t \to +\infty$, one to $(0, -\infty, 1)$, and one to $(1, 0, +\infty)$. These and other experiments suggest that

all solutions except for equilibria must eventually approach one of the straight lines $(X, Y) = (1, 0)$ or $(Y, Z) = (1, 0)$.

It is far from clear, analytically, why the solutions behave in this way. For, simply putting $X = 1, Y = 0$ yields

$$\dot{X} = hX = h, \qquad \dot{Y} = -2Y = 0, \qquad \dot{Z} = -1 + hZ,$$

which implies that X must continue to increase, as well as Z. (Similarly for other cases.) But Figures 18 shows that there are damped oscillations as the constant values 0 and 1 are approached. It is clear that the term $Y(Z-1)$ cannot be neglected, since as $Y \to 0$, Z tends to infinity and $Y(Z-1)$ tends to a certain non-zero value, which cancels hX out, thus $\dot{X} \approx 0$.

We find it difficult to rigorously prove unboundedness of the orbits. We therefore assume, for example, that $X \to \infty, Y \to 1, Z \to 0$ as $t \to \infty$. Then, from this rough assumption, we will derive much more accurate asymptotic behaviour.

Assuming that $h > 0, k > 0$, we here describe the asymptotic structure of those solutions of (4) that approach straight lines. We suppose that X increases indefinitely while Y approaches 1 and Z approaches 0. (A corresponding description exists for the other cases where, e.g., $|Z|$ increases indefinitely while Y approaches 0 and X approaches 1. Though similar, this will not be identical, since there is no longer an invariant map, $(X, Y, Z, t) \leftrightarrow (1-Z, 1-Y, 1-X, T-t)$ as occurs for the equations when $h = k = 0$. Details of this are not given here.)

Eliminating t in (4) gives

$$\frac{\mathrm{d}Y}{\mathrm{d}X} = \frac{-Z(X-1) - kY}{Y(Z-1) + hX}, \qquad \frac{\mathrm{d}Z}{\mathrm{d}X} = \frac{X(Y-1) + hZ}{Y(Z-1) + hX}. \tag{13}$$

Now introduce a small parameter Δ and set

$$X = \xi/\Delta, \qquad Y = 1 + \Delta\eta_1 + \Delta^2\eta_2 + \cdots, \qquad Z = \Delta\zeta_1 + \Delta^2\zeta_2 + \cdots,$$

anticipating that X is large, Y is close to 1, and Z is small. Further, in the spirit of "two-timing", suppose that η_1, η_2 etc. and ζ_1, ζ_2 etc. are functions of

the *two* variables X and ξ, regarded as independent. (Here, X is the "fast" variable and ξ the "slow" one.) Thus,

$$\frac{\mathrm{d}Y}{\mathrm{d}X} = \Delta\left(\frac{\partial\eta_1}{\partial X}\right) + \Delta^2\left(\frac{\partial\eta_1}{\partial\xi} + \frac{\partial\eta_2}{\partial X}\right) + O(\Delta^3), \tag{14}$$

$$\frac{\mathrm{d}Z}{\mathrm{d}X} = \Delta\left(\frac{\partial\zeta_1}{\partial X}\right) + \Delta^2\left(\frac{\partial\zeta_1}{\partial\xi} + \frac{\partial\zeta_2}{\partial X}\right) + O(\Delta^3). \tag{15}$$

Their respective right-hand sides in (13) are

$$\Delta\left(-\frac{\zeta_1}{h} - \frac{k}{h\xi}\right) + \Delta^2\left[\frac{(h-1)\zeta_1}{h^2\xi} - \frac{k}{h^2\xi^2} - \frac{k\eta_1}{h\xi} - \frac{\zeta_2}{h}\right] + O(\Delta^3),$$
$$\Delta\frac{\eta_1}{h} + \Delta^2\left(\frac{\eta_2}{h} + \frac{\zeta_1}{\xi} + \frac{\eta_1}{h^2\xi}\right) + O(\Delta^3).$$

Accordingly, at $O(\Delta)$, we have

$$\frac{\partial\eta_1}{\partial X} = -\frac{\zeta_1}{h} - \frac{k}{h\xi}, \qquad \frac{\partial\zeta_1}{\partial X} = \frac{\eta_1}{h},$$

and integration gives

$$\eta_1 = P(\xi)\cos\left[\frac{X}{h} + \Theta(\xi)\right], \qquad \zeta_1 = -\frac{k}{\xi} + P(\xi)\sin\left[\frac{X}{h} + \Theta(\xi)\right]$$

for some functions P and Θ to be determined.

At next order,

$$\frac{\partial\eta_1}{\partial\xi} + \frac{\partial\eta_2}{\partial X} = \frac{(h-1)\zeta_1}{h^2\xi} - \frac{k}{h^2\xi^2} - \frac{k\eta_1}{h\xi} - \frac{\zeta_2}{h},$$
$$\frac{\partial\zeta_1}{\partial\xi} + \frac{\partial\zeta_2}{\partial X} = \frac{\eta_2}{h} + \frac{\zeta_1}{\xi} + \frac{\eta_1}{h^2\xi},$$

which yield

$$\frac{\partial\eta_2}{\partial X} + \frac{k}{h\xi^2} + \frac{\zeta_2}{h} = \left(\frac{h-1}{h^2\xi} + \frac{\mathrm{d}\Theta}{\mathrm{d}\xi}\right)P\sin\left[\frac{X}{h} + \Theta(\xi)\right] - \left(\frac{\mathrm{d}P}{\mathrm{d}\xi} + \frac{k}{h\xi}P\right)\cos\left[\frac{X}{h} + \Theta(\xi)\right],$$
$$\frac{\partial\zeta_2}{\partial X} + \frac{2k}{\xi^2} - \frac{\eta_2}{h} = \left(\frac{1}{h^2\xi} - \frac{\mathrm{d}\Theta}{\mathrm{d}\xi}\right)P\cos\left[\frac{X}{h} + \Theta(\xi)\right] + \left(-\frac{\mathrm{d}P}{\mathrm{d}\xi} + \frac{1}{\xi}P\right)\sin\left[\frac{X}{h} + \Theta(\xi)\right].$$

Now, if the right-hand sides were zero, integration with respect to X would give the general solution

$$\eta_2 = \frac{2hk}{\xi^2} + Q(\xi)\cos\left[\frac{X}{h} + \Phi(\xi)\right], \qquad \zeta_2 = -\frac{k}{\xi^2} + Q(\xi)\sin\left[\frac{X}{h} + \Phi(\xi)\right]$$

for some slowly-varying functions Q, Φ. However, since there are terms on the right-hand side with this same periodicity on the "fast" scale X, secular growth proportional to $X\cos[X/h+\Phi]$ and to $X\sin[X/h+\Phi]$ must normally occur. To suppress this unwanted growth, which would cause the asymptotic expansions to become disordered, one must restrict the choice of P and Θ. Reduction to a single second-order equation yields

$$\frac{\partial^2}{\partial X^2}\left(\zeta_2+\frac{k}{\xi^2}\right)+\frac{1}{h^2}\left(\zeta_2+\frac{k}{\xi^2}\right)=\left(\frac{h-2}{h^2\xi}+2\frac{\mathrm{d}\Theta}{\mathrm{d}\xi}\right)\frac{1}{h}P\sin\left[\frac{X}{h}+\Theta(\xi)\right] + \left(-2\frac{\mathrm{d}P}{\mathrm{d}\xi}+\frac{h-k}{h\xi}P\right)\frac{1}{h}\cos\left[\frac{X}{h}+\Theta(\xi)\right]$$

from which it is clear that one must choose

$$\frac{\mathrm{d}P}{\mathrm{d}\xi}=\frac{h-k}{2h\xi}P, \qquad \frac{\mathrm{d}\Theta}{\mathrm{d}\xi}=\frac{2-h}{2h^2\xi}.$$

The same equations for P and Θ also result from the corresponding second-order equation for η_2.

Integration gives

$$P(\xi)=P_0|\xi|^{\frac{h-k}{2h}}, \qquad \Theta=\frac{2-h}{2h^2}\log|\xi|+\text{constant},$$

where P_0 is any constant. Thus, provided $k>h$, the amplitude of oscillations of η_1 and ζ_1 decreases algebraically with ξ. Also, ζ_1, but not η_1, has a non-oscillatory part $-k/\xi$, that decays as the magnitude of ξ increases. These features are evident in the particular solutions shown in Figures 17 and 18.

To express the results in terms of time t, one must integrate

$$\frac{\mathrm{d}X}{\mathrm{d}t}=Y(Z-1)+hX=(1+\Delta\eta_1+\cdots)(-1+\Delta\zeta_1+\Delta^2\zeta_2+\cdots)+hX$$
$$=hX-1+O(\Delta)$$

to get

$$X=X_0\exp(ht)+h^{-1}+O(\Delta), \qquad (X_0 \text{ arbitrary}),$$

where, by assumption, the term h^{-1} is small compared with $|X_0|\exp(ht)$. It

follows that

$$\begin{aligned} Y &= 1 + \Delta\eta_1 + \cdots \\ &= 1 + \Delta P_0 |\xi|^{\frac{h-k}{2h}} \cos\left[\frac{X}{h} + \Theta(\xi)\right] + \cdots \\ &= 1 + P_0 \Delta^{\frac{3h-k}{2h}} |X|^{\frac{h-k}{2h}} \cos\left[\frac{X_0}{h}\exp(ht) + \frac{1}{h^2} + \Theta(\xi)\right] + \cdots \\ &= 1 + P_1 \exp\left(\frac{(h-k)t}{2}\right) \cos\left[\exp(h(t-t_0)) + \Theta(\xi)\right] + \cdots \end{aligned}$$

where P_1 and t_0 are arbitrary constants, and the term in h^{-2} within the cosine may be absorbed into the further arbitrary constant that appears in Θ. Also, on replacing ξ by ΔX, the slowly-varying function Θ may be seen to vary as $t(2-h)/2h$ when X is sufficiently large.

Similarly,

$$\begin{aligned} Z &= \Delta\zeta_1 + \cdots \\ &= \Delta\left[-\frac{k}{\xi} + P(\xi)\sin\left[\frac{X}{h} + \Theta(\xi)\right]\right] + \cdots \\ &= \frac{-k}{X} + P_0 \Delta^{\frac{3h-k}{2h}} |X|^{\frac{h-k}{2h}} \sin\left[\frac{X_0}{h}\exp(ht) + \frac{1}{h^2} + \Theta(\xi)\right] + \cdots \\ &= \frac{-k}{h^{-1} + X_0\exp(ht)} + P_1 \exp\left(\frac{(h-k)t}{2}\right) \sin\left[\exp(h(t-t_0)) + \Theta(\xi)\right] + \cdots . \end{aligned}$$

These solutions are characterised by a non-oscillatory term in Z that decays exponentially as $\exp(-ht)$ when t is sufficiently large; and by rapid small oscillations of both Y and Z, with frequency that increases exponentially with time, and amplitude that decays exponentially like $\exp((h-k)t/2)$, (where $k > h > 0$ by assumption). These features are broadly replicated in the specific cases that have been computed. Figure 19 shows the time sequence of the orbit of (4) at $h = 0.3, k = 2.0$ starting at $(X, Y, Z) = (10, 10, 10)$. It convinces us of the validity of our asymptotic analysis.

6. Case C

In this section we consider the case $h < 0, k > 0$. Both h and k play a role of a damping factor, and $2h - k < 0$ holds for all $h < 0$ and $k > 0$. This case

has no unbounded solution, as we can prove the existence of an ellipsoid into which all orbits eventually fall. We apply a standard argument using Lyapunov functions. See, e.g., [23, Sect. 14.2], in which a similar argument is applied to the well-known Lorenz system.

Proposition 1. *Assume $h < 0$ and $k > 0$. Let $V : \mathbb{R}^3 \to \mathbb{R}$ be defined by*

$$V(X, Y, Z) = (X - 2)^2 + 2(Y - 1/2)^2 + (Z + 1)^2. \tag{16}$$

Then, there exists an $a > 0$ such that the set

$$\{V \le a\} := \{(X, Y, Z) \mid V(X, Y, Z) \le a\}$$

is positively invariant and all the orbits starting from $\{V > a\}$ enter the set $\{V \le a\}$ in finite time (and remain there thenceforth).

Proof. Differentiating along the orbit, we obtain

$$\begin{aligned}
\dot{V} &= \frac{\mathrm{d}}{\mathrm{d}t} V(X(t), Y(t), Z(t)) \\
&= 2\left[hX^2 - 2kY^2 + hZ^2 - (1 + 2h)X + (k + 2)Y + (h - 1)Z\right] \\
&= -2\left[-h\left(X - \frac{2h + 1}{2h}\right)^2 + 2k\left(Y - \frac{k + 2}{4k}\right)^2 - h\left(Z - \frac{1 - h}{2h}\right)^2 + \tilde{C}\right],
\end{aligned}$$

where

$$\tilde{C} = h\left(\frac{2h + 1}{2h}\right)^2 - 2k\left(\frac{k + 2}{4k}\right)^2 + h\left(\frac{h - 1}{2h}\right)^2.$$

If $h < 0$ and $k > 0$, then the set $\{(X, Y, Z) \mid \dot{V} = 0\}$ is an ellipsoid, and $\dot{V} < 0$ holds outside this ellipsoid. One can choose sufficiently large a such that $\{(X, Y, Z) \mid V < a\}$ contains $\{(X, Y, Z) \mid \dot{V} \ge 0\}$. Then $\dot{V}$ is strictly negative for any $(X, Y, Z) \in \{(X, Y, Z) \mid V \ge a\}$, and the orbit of (X, Y, Z) must enter $\{(X, Y, Z) \mid V \le a\}$. □

This theorem proves that all the orbits are bounded. Further information about asymptotic behaviour is difficult to obtain. As the following theorem demonstrates, asymptotic stability of the origin can be proved for a large class of (h, k).

Theorem 1. *$L(X,Y,Z) = X^2 + 2Y^2 + Z^2$ is a Lyapunov function for (4) if*

$$h < -\frac{1}{2} \qquad \textit{and} \qquad k > \frac{2-5h}{8h^2-2}. \tag{17}$$

Accordingly, the origin is globally asymptotically stable if this condition is satisfied.

Proof. We have

$$\frac{1}{2}\frac{\mathrm{d}}{\mathrm{d}t}L(X(t),Y(t),Z(t)) = hX^2 - 2kY^2 + hZ^2 - XY + 2YZ - ZX.$$

The quadratic form in the right hand side is negative-definite if and only if (17) holds. Indeed, the symmetric matrix A, which generates the quadratic form,

$$A = \begin{pmatrix} h & -1/2 & -1/2 \\ -1/2 & -2k & 1 \\ -1/2 & 1 & h \end{pmatrix},$$

is negative-definite if and only if the leading principal minors of $-A$ are all positive. One can derive (17) by a simple calculation.

Obviously, L is non-negative, and $L = 0$ if and only if $(X,Y,Z) = (0,0,0)$. If (17) holds, then $\dot{L}$ is non-positive and it vanishes only at the origin. Therefore L is a Lyapunov function. □

Figure 20 shows the parameter region (17) as well as several bifurcation curves which are explained later. The linearised matrix of (4) at the origin is (12). If applied to this matrix, the Routh-Hurwitz criterion (see for instance [24, Chap. XV]) implies that the origin is linearly stable if and only if $h < 0$ and $k > h^{-2}$. The set $\{(h,k) \mid kh^2 = 1\}$ is the curve labelled `BP` in Figure 20, from which equilibria bifurcate.

Behaviour of a solution is not obvious if (17) is not satisfied. For instance, since the periodic orbit at $(h,k) = (0,0)$ is hyperbolic, it persists under a small perturbation. Also, the nontrivial equilibrium $(X,Y,Z) = (1,1,1)$ for (10) persists for the same reason. Therefore the global asymptotic stability of the origin does not hold in a neighbourhood of $(h,k) = (0,0)$. There exist at most

five equilibria including the origin. The curves labelled LP1 and LP2 in Figure 20 consist of limit points of nontrivial equilibrium, in other words, they consist of saddle-node bifurcation points at which two nontrivial equilibria collide. A sample of diagram when $h = -1$ is drawn in Figure 20(b). When (h, k) is inside the region bounded by the coordinate axes and the curve labelled LP1, there are five equilibria, and two of four nontrivial equilibria are stable. The k-axis is tangent to LP1 at $(h, k) = (0, 1)$, which is the Bogdanov-Takens bifurcation point. Further study requires more analysis. We leave it to the forthcoming paper.

7. Final remarks

A system of damped and forced equations (4) is introduced. If $h < 0, k < 0$, three chaotic attractors of different nature can exist. Two of them arise as a consequence of period-doubling cascades. The third is related to homoclinic bifurcations and period-doubling cascades.

If $h > 0, k > 0$, no chaotic orbit is found and unbounded orbits are dominant. We are unable to prove the unboundedness of orbits, but we can associate them with asymptotic analysis. The result predicts orbits' properties accurately, and numerical data support it well.

Other cases seem to offer interesting challenges: we will study them in the forthcoming paper.

Acknowledgments

T.M. is supported by the Grant-in-Aid for JSPS Fellow No. 24·5312. H.O. is partially supported by JSPS KAKENHI 24244007.

References

[1] A.D.D. Craik, H. Okamoto, A three-dimensional autonomous system with unbounded 'bending' solutions, Physica D 164 (2002) 168–186. doi:10.1016/S0167-2789(02)00372-X.

[2] A.D.D. Craik, Time-dependent solutions of the Navier-Stokes equations for spatially-uniform velocity gradients, Proc. Roy. Soc. Edinburgh Sect. A 124 (1994) 127–136. doi:10.1017/S0308210500029231.

[3] S. Anastassiou, S. Pnevmatikos, T. Bountis, Quadratic vector fields equivariant under the D_2 symmetry group, Internat. J. Bifur. Chaos Appl. Sci. Engrg. 23 (2013) 1350017. doi:10.1142/S021812741350017X.

[4] G.N. Chechin, D.S. Ryabov, Three-dimensional chaotic flows with discrete symmetries, Phys. Rev. E 69 (2004) 036202. doi:10.1103/PhysRevE.69.036202.

[5] W. Liu, G. Chen, A new chaotic system and its generation, Internat. J. Bifur. Chaos Appl. Sci. Engrg. 13 (2003) 261–267. doi:10.1142/S0218127403006509.

[6] J. Llibre, M. Messias, P.R. da Silva, On the global dynamics of the Rabinovich system, J. Phys. A: Math. Theor. 41 (2008) 275210.

[7] I. Pehlivan, I.M. Moroz, S. Vaidyanathan, Analysis, synchronization and circuit design of a novel butterfly attractor, J. Sound and Vibration 333 (2014) 5077–5096.

[8] T. Miyaji, H. Okamoto, A.D.D. Craik, A four-leaf chaotic attractor of a three-dimensional dynamical system, Internat. J. Bifur. Chaos Appl. Sci. Engrg. 25 (2015) 1530003. doi:10.1142/S0218127415300037.

[9] A.D.D. Craik, Wave Interactions and Fluid Flows, Cambridge Monographs on Mechanics, Cambridge University Press, 1985.

[10] A.D.D. Craik, H. Okamoto, H.R. Allen, Second-harmonic resonance with parametric excitation and damping, in: J. L. Lumley (Ed.), Fluid Mechanics and the Environment: Dynamical Approaches, Vol. 566 of Lect. Notes in Phys., Springer Berlin Heidelberg, 2001, pp. 63–89. doi:10.1007/3-540-44512-9_4.

[11] G.K. Forster, A.D.D. Craik, The stability of three-dimensional time-periodic flows with ellipsoidal stream surfaces, J. Fluid Mech. 324 (1996) 379–391. doi:10.1017/S0022112096007963.

[12] D.W. Hughes, M.R.E. Proctor, Chaos and the effect of noise in a model of three-wave mode coupling, Physica D 46 (1990) 163–176. doi:10.1016/0167-2789(90)90034-M.

[13] F.T. Smith, P.A. Stewart, The resonant-triad nonlinear interaction in boundary-layer transition, J. Fluid Mech. 179 (1987) 227–252. doi:10.1017/S0022112087001502.

[14] J.-M. Wersinger, J.M. Finn, E. Ott, Bifurcation and "strange" behavior in instability saturation by nonlinear three-wave mode coupling, Phys. Fluids 23 (1980) 1142–1154. doi:10.1063/1.863116.

[15] İ Pehlivan, Four-scroll stellate new chaotic system, Optoelect. Adva. Mater. 5 (2011) 1003–1006.

[16] L. Euler, Theoria Motus Corporum Solidorum seu Rigidorum, Griefswald, 1765, (Also *L. Euler, Opera Omnia* Ser. II, **3** and **4**.).

[17] T. Miyaji, H. Okamoto, A computer-assisted proof of existence of a periodic solution, Proc. Japan Acad. Ser. A 90 (2014) 139–144. doi:10.3792/pjaa.90.139.

[18] E.J. Doedel, B.E. Oldeman, AUTO-07P: Continuation and Bifurcation Software for Ordinary Differential Equations, Concordia University, Montreal, Canada (January 2012).
URL `http://cmvl.cs.concordia.ca/auto/`

[19] J.-P. Eckmann, D. Ruelle, Ergodic theory of chaos and strange attractors, Rev. Mod. Phys. 57 (1985) 617–656. doi:10.1103/RevModPhys.57.617.

[20] M.J. Feigenbaum, Quantitative universality for a class of nonlinear transformations, J. Stat. Phys. 19 (1978) 25–52. doi:10.1007/BF01020332.

[21] L.P. Šil'nikov, A case of the existence of a countable number of periodic motions, Soviet Math. Dokl. 6 (1965) 163–166.

[22] T. Miyaji, H. Okamoto, A.D.D. Craik, Three-dimensional forced-damped dynamical systems with rich dynamics: bifurcations, chaos and unbounded solutions II, unpublished results.

[23] M.W. Hirsch, S. Smale, R.L. Devaney, Differential Equations, Dynamical Systems & An Introduction to Chaos, Elsevier Academic Press, San Diego, 2004.

[24] F.R. Gantmacher, Theory of Matrices, Volume 2, Chelsea, 1959.

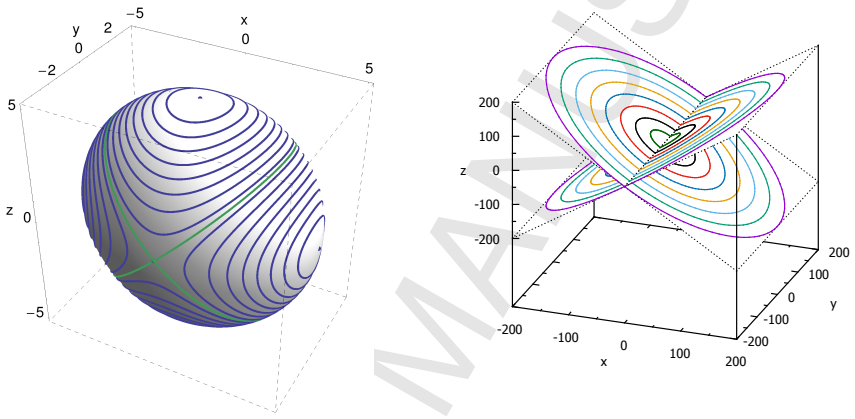

(a) $R = 10$ (b) $x = \pm z$

Figure 1: (a) Orbits of (5) on $x^2 + 2y^2 + z^2 = 10^2$. The green orbits are heteroclinic, the blue ones are closed. (b) Heteroclinic orbits on the invariant set $x = \pm z$.

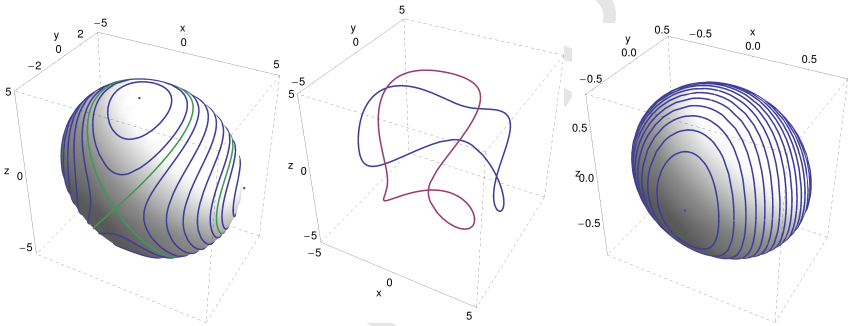

(a) $R = 10$ (b) Two orbits in (a) (c) $R = 0.8$

Figure 2: Orbits of (7) on $X^2 + 2Y^2 + Z^2 = R^2$. The green orbits in (a) are homoclinic.

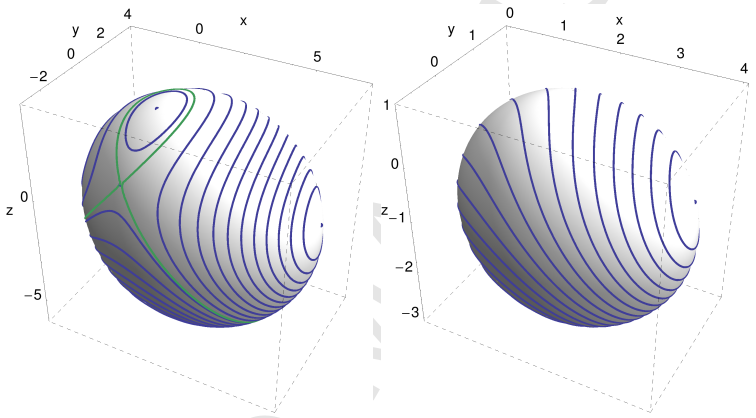

(a) $R = 10$ (b) $R = 2$

Figure 3: Orbits of (11) on the ellipsoid $(X-2)^2 + 2(Y-1/2)^2 + (Z+1)^2 = R^2$.

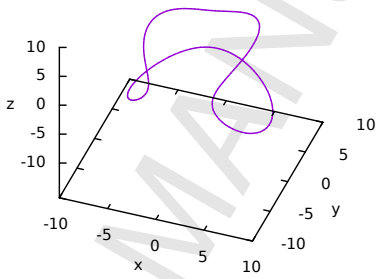

Figure 4: Unstable periodic orbit of (10). It passes through $(X, Y, Z) \approx (8.043, 0.5, -7.043)$.

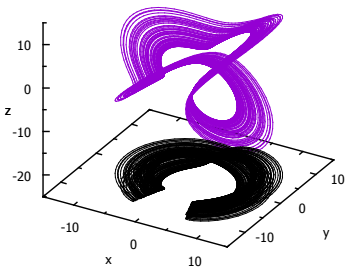

(a) $IC = (4, -6, 0)$, $h = -1.5, k = -1$

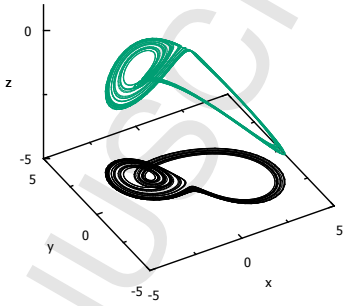

(b) $IC = (-2, 3, -1)$, $h = -1.5, k = -1.1$

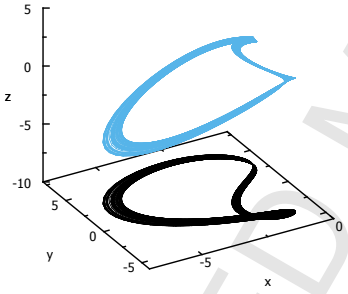

(c) $IC = (-1, 5, 0), h = -2, k = -1.125$

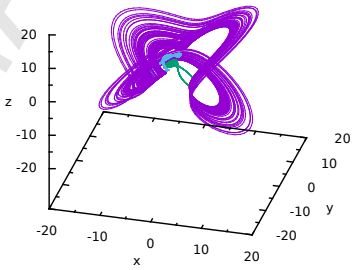

(d) All together for $h = -1.97, k = -1.1262$

Figure 5: Orbits of (4) for $800 < t < 1000$ and their projections onto the XY-plane. IC means the initial condition, i.e., $IC = (X(0), Y(0), Z(0))$.

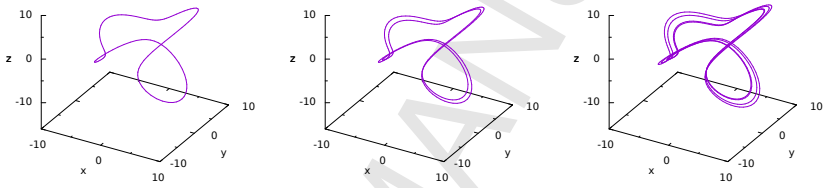

(a) $k = -1.1$ (b) $k = -1.04$ (c) $k = -1.022$

Figure 6: Stable limit cycles of (4) for $h = -1.5$. These orbits are computed from the initial value $(X_0, Y_0, Z_0) = (4, -6, 0)$.

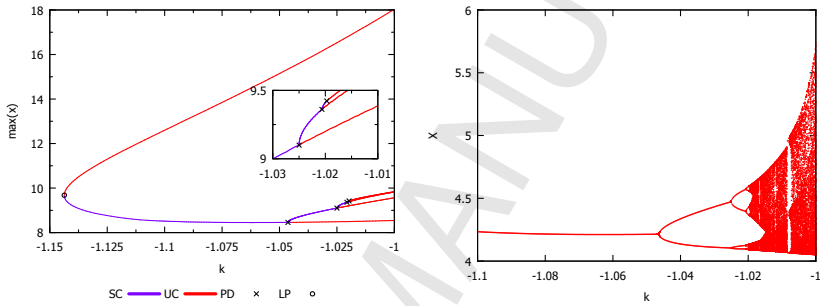

(a) (b)

Figure 7: (a) Bifurcation diagram of (4) for $h = -1.5$ (b) Orbit diagram of (4) with $h = -1.5$, continued from the limit cycle at $k = -1.1$ in Fig 6(a). The vertical axis is the X-coordinate of the intersection of an orbit and the Poincaré section $\{Z = 0, \dot{Z} < 0\}$.

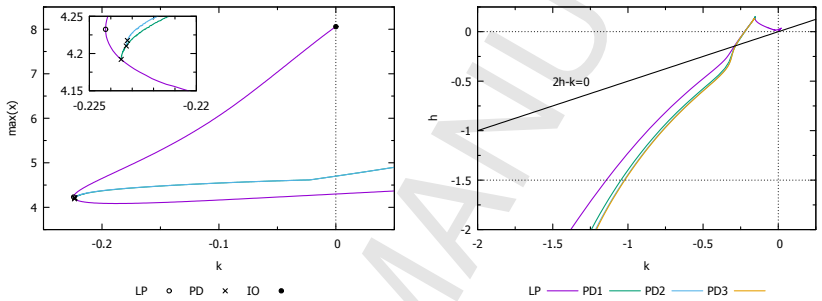

(a) (b)

Figure 8: (a) Bifurcation diagram of (4) with $h = 0$. `IO` means the periodic orbit in Figure 4. (b) Two-parameter bifurcation diagram of (4). Each curve is a continuation of the bifurcation point shown in Figure 8(a). `PD2` and `PD3` are very close to each other.

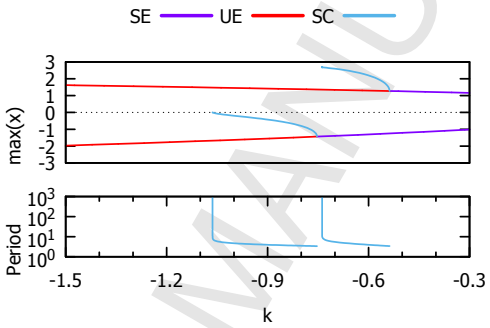

Figure 9: One-parameter bifurcation diagram of (4) with $h = -1.5$. The upper figure shows k versus $\max(X)$ and the lower shows k versus the period of the limit cycle.

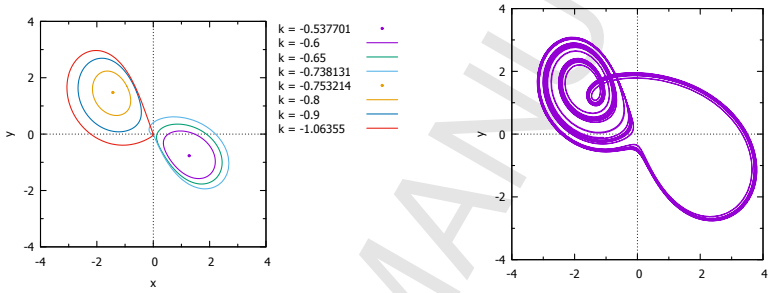

(a) (b)

Figure 10: (a) Periodic orbits of (4) at $h = -1.5$ bifurcating from an equilibrium and approaching a homoclinic orbit. (b) An attractor at $k = -1.07$ which passes near a vestige of a homoclinic orbit. Both figures are projections onto the XY-plane

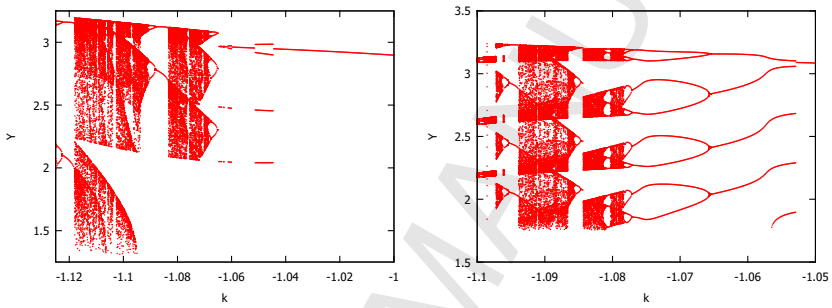

(a) $h = -1.5$ (b) $h = -1.7$

Figure 11: Orbit diagrams of (4) for $h = -1.5, -1.7$. $IC = (-2, 3, -1)$. The vertical axis is the Y-coordinate on the Poincaré section $\{X = -2, \dot{X} < 0\}$

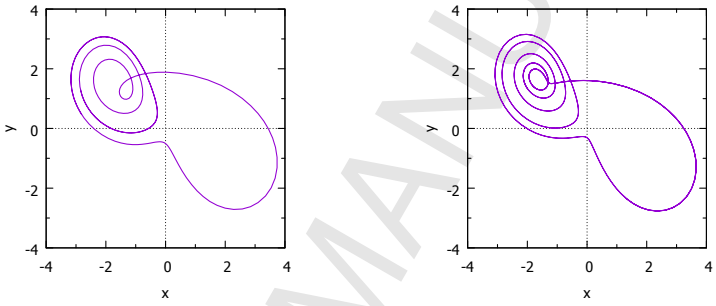

(a) $(h, k) = (-1.5, -1.065)$ (b) $(h, k) = (-1.7, -1.06)$

Figure 12: Stable limit cycles of (4) projected onto XY-plane. These orbits are computed from $IC = (-2, 3, -1)$.

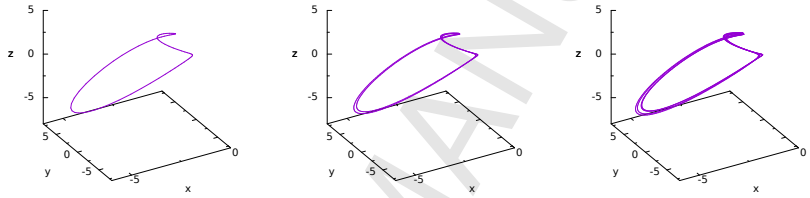

(a) $k = -1.14$ (b) $k = -1.135$ (c) $k = -1.1305$

Figure 13: Stable limit cycles of (4) with $h = -2.0$. They are obtained from $(X, Y, Z) = (-1, 5, 0)$.

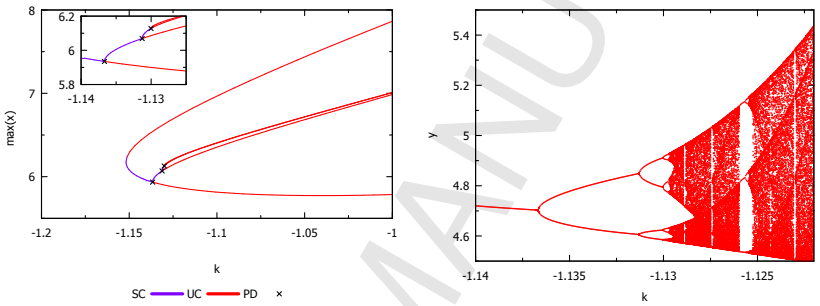

(a) (b)

Figure 14: (a) One-parameter bifurcation diagram of (4) at $h = -2.0$. The vertical axis is $\max(Y)$. (b) Orbit diagram of (4) at $h = -2.0$. The vertical axis is the Y-coordinate of the intersection of an orbit and the Poincaré section $\{Z = 0, \dot{Z} < 0\}$.

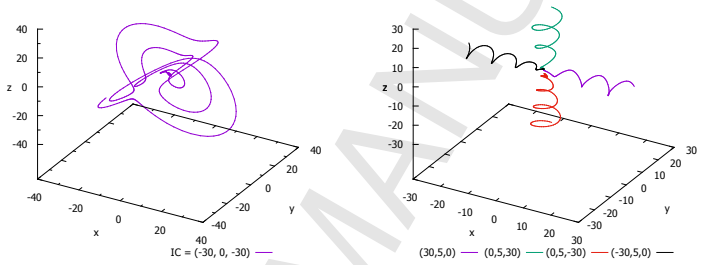

(a) (b)

Figure 15: Orbits which converge to an equilibrium of (4) with $(h, k) = (-1.5, -0.1)$.

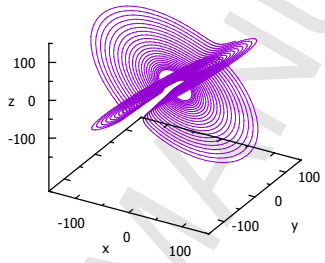

Figure 16: An orbit of (4) growing without bound, with $(h, k) = (-1.5, -1.0)$ starting at $IC = (20, 20, 20)$.

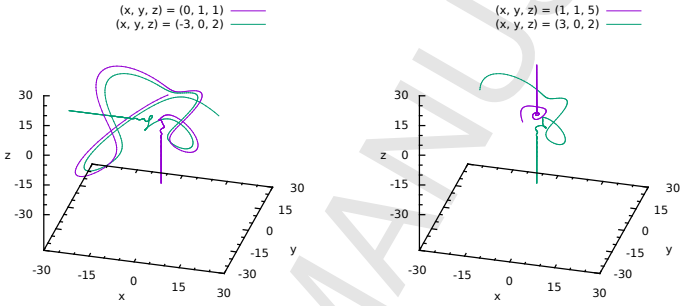

(a) (b)

Figure 17: Orbits of (4) at $h = 0.3, k = 2.0$ (a) those starting at $(X, Y, Z) = (0, 1, 1)$ and $(-3, 0, 2)$. Both orbits are computed for $-2.5 \leq t \leq 20$ and plotted in the cube $[-30, 30]^3$. (b) those starting at $(X, Y, Z) = (1, 1, 5)$ and $(3, 0, 2)$. Both are computed for $-2 \leq t \leq 20$ and plotted in the same cube $[-30, 30]^3$.

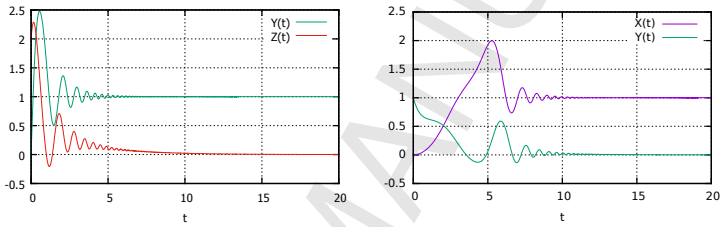

(a) (b)

Figure 18: Time sequence of the orbit for (4) at $h = 0.3, k = 2.0$. (a) orbit from $(X, Y, Z) = (-3, 0, 2)$. (b) orbit from $(X, Y, Z) = (0, 1, 1)$.

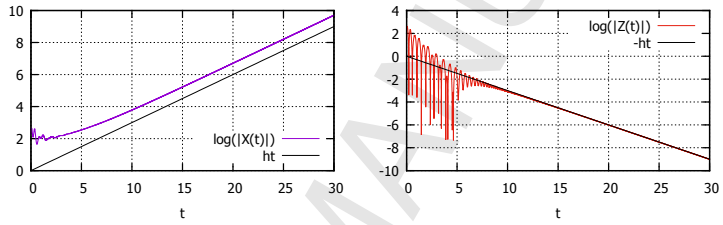

(a) (b)

Figure 19: Time sequence of $\log|X(t)|$ and $\log|Z(t)|$ of the orbit of (4) at $h = 0.3, k = 2.0$ starting at $(X, Y, Z) = (10, 10, 10)$. (a) t versus $\log|X(t)|$. (b) t versus $\log|Z(t)|$.

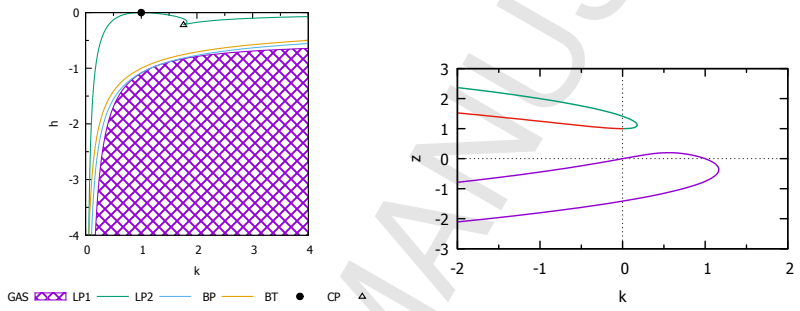

(a) (b)

Figure 20: (a) Two-parameter bifurcation diagram of equilibria for (4) in Case C. The origin is globally asymptotically stable in the chequered region `GAS`. `LP1` and `LP2` are curves of limit points of nontrivial equilibria. `BP` is the curve of bifurcation points of the origin. (b) Equilibria for $h = -1$.